Available online at www.sciencedirect.com
SCIENCE DIRECT®
Journal of Photochemistry and Photobiology A: Chemistry 157 (2003) 247–256
Journal of Photochemistry and Photobiology A:Chemistry
www.elsevier.com/locate/jphotochem

Gas phase elemental mercury: a comparison of LIF detection techniques and study of the kinetics of reaction with the hydroxyl radical

D. Bauer, L. D'Ottone, P. Campuzano-Jost, A.J. Hynes*

Division of Marine and Atmospheric Chemistry, Rosenstiel School of Marine and Atmospheric Science, University of Miami, 4600 Rickenbacker Causeway, Miami, FL 33149, USA

Received 24 June 2002; received in revised form 2 August 2002; accepted 3 September 2002

Abstract

We have examined the sensitivity of single and sequential two-photon laser-induced fluorescence (LIF) techniques for the detection of elemental mercury, Hg(0), in the gas phase. Single photon LIF involves excitation of the 6^3P_1–6^1S_0 transition at 253.7 nm, followed by observation of resonance fluorescence. Sequential two-photon techniques follow the initial 6^3P_1–6^1S_0 excitation with a second excitation step to either the 7^1S_0 or 7^3S_1 levels followed by observation of blue or red shifted fluorescence. We have examined four variants of these approaches which all exceed the sensitivity of single photon LIF. The most sensitive detection approach involves the initial 253.7 nm excitation followed by excitation of the 7^1S_0–6^3P_1 transition at 407.8 nm. Fluorescence is observed on the 6^1P_1–6^1S_0 transition at 184.9 nm. Using this approach, our limits of detection are 0.1 ng m^{-3} with a 10 s integration time in air. We have also examined the effects of saturation, quenching and line-width on detection sensitivity. We have used the pulsed laser photolysis–pulsed laser-induced fluorescence (PLP-PLIF) technique to study the kinetics of the reaction of elemental mercury with the hydroxyl radical under atmospheric conditions at 298 K. We see no evidence for reaction and obtain an upper limit of 1.2×10^{-13} cm^3 $molecule^{-1}$ s^{-1} for the rate coefficient.

Keywords: Laser-induced fluorescence; Elemental mercury; Pulsed laser photolysis

1. Introduction

A detailed understanding of the role of mercury in the environment is a critical issue from a human health perspective. Direct exposure to mercury is primarily through the ingestion of methylmercury from fish consumption and the National Academy of Sciences report "Toxicological Effects of Methylmercury" [1] estimated that more than 60,000 US children are born each year with a risk of damaged nervous systems from methylmercury exposure in the womb. A knowledge of the rates and mechanisms of emission, deposition and chemical transformation of elemental mercury is essential in understanding the cycling of mercury in aquatic and terrestrial ecosystems. Hg(0) concentrations range from typical values of 1–4 ng m^{-3} (1 ng m^{-3} $\sim 3 \times 10^6$ atoms cm^{-3} $\sim$ 120 ppq (parts per quadrillion) at SATP) in remote areas [2] and can reach more than 1000 ng m^{-3} near mercury sources [3]. Until recently, Hg(0) was thought to be unreactive in the gas phase under atmospheric conditions, having a lifetime of approximately one year [4,5] although it was noted that this estimate was highly uncertain. New measurements of the rapid depletion of atmospheric mercury in the arctic have demonstrated that, at least under some circumstances, mercury can undergo fast atmospheric cycling [6,7]. These depletion events correlate well with the depletion of atmospheric ozone that appears to be triggered by the photolysis of labile halogen species released from the snowpack after the arctic sunrise. The implications of this for atmospheric mercury chemistry on a global scale are unclear because the precise mechanism of the arctic depletion events is not known and very little data is available for rate coefficients of Hg(0) with halogens.

Atmospheric chemical transformation in the troposphere is dominated by hydroxyl radical (OH) chemistry but the reaction of Hg with OH

$$\mathrm{Hg(0) + OH \rightarrow products} \quad (1)$$

has been discounted as a likely oxidation route for Hg(0) [8] primarily because a direct reaction, i.e.

$$\mathrm{Hg + OH \rightarrow HgO + H}, \quad \Delta H = +90\ \mathrm{kJ\ mole^{-1}} \quad (1a)$$

is highly endothermic. However, a potential alternate route for such a reaction is via a weakly bound intermediate HgOH which then reacts with O_2, i.e.

$$\mathrm{Hg + OH \leftrightarrow HgOH} \quad (1b)$$

* Corresponding author. Fax: +1-305-3614689.
E-mail address: ahynes@rsmas.miami.edu (A.J. Hynes).

1010-6030/03/$ – see front matter © 2003 Elsevier Science B.V. All rights reserved.
doi:10.1016/S1010-6030(03)00065-0

$$HgOH + O_2 \rightarrow HgO + HO_2 \quad (2)$$

net

$$Hg + OH + O_2 \rightarrow HgO + HO_2, \quad \Delta H = -118\,kJ\,mole^{-1} \quad (3)$$

a process which is exothermic overall, with the exothermicity of the individual steps depending on the binding energy of HgOH.

As part of a program to study the gas phase atmospheric chemistry of mercury we have examined the sensitivity of single and sequential two-photon laser-induced fluorescence (LIF) detection techniques for gas phase Hg(0) under atmospheric conditions. These techniques combine extremely high detection sensitivity, selectivity and very fast time response. Each approach involves an initial laser excitation of the 6^3P_1–6^1S_0 transition at 253.7 nm. In the sequential two-photon LIF technique, this is followed by excitation with a second laser to either the 7^1S_0 or 7^3S_1 levels. Either blue or red shifted laser-induced fluorescence is then monitored with a photomultiplier tube (PMT). In previous work, we have described the analytical application of the most sensitive approach [9]. In this work, we compare sensitivities of each detection scheme and the effects of saturation, quenching and excitation line-width on detection sensitivity. In addition, we present some results on the kinetics of the reaction of the hydroxyl radical with Hg(0) using the pulsed laser photolysis–pulsed laser-induced fluorescence (PLP-PLIF) technique.

2. Experimental

2.1. Spectroscopy and detection sensitivity

The experimental setup has been described in detail [9] and features the ability to synchronize two independently tunable laser systems, the generation and measurement of known concentrations of mercury and the simultaneous detection of two fluorescence wavelengths. A brief description relevant to this work is included below.

The excitation beams were generated by two, 10 Hz laser systems. They were combined using a dichroic mirror and propagated collinearly through a gas mixture containing a known concentration of mercury. Mixtures of elemental mercury and N_2 were produced by flowing a controlled nitrogen flow over an uncalibrated permeation tube. The mercury concentration could be further diluted by pure nitrogen to reach the wide range of concentrations, from 1 to 14,000 ng m^{-3}, used in these measurements. Mercury concentrations were measured with a commercial mercury analyzer (Tekran 2537A) which was able to measure concentrations in the range of 0.1–1000 ng m^{-3} with a time resolution of 5 min [10]. Where higher concentrations were used they were calculated by extrapolating the concentration from values below 1000 ng m^{-3} to higher values based on changes in flows and dilution. The fluorescence cell, which was constructed of Pyrex, had four mutually perpendicular side arms with quartz windows. The two laser beams passed collinearly through two side arms across the direction of gas flow. Fluorescence was detected through the other two side arms, perpendicular to the excitation beams using quartz and CaF lenses. The first step in all experiments was excitation of the 6^3P_1 level using the 6^3P_1–6^1S_0 transition at 253.7 nm. For single photon LIF measurements, resonance fluorescence was detected by a PMT with a 254 nm interference filter. In sequential two-photon measurements, the initial excitation to the 6^3P_1 level was followed by excitation of either the 7^1S_0 level via the 7^1S_0–6^3P_1 transition at 407.8 nm or the 7^3S_1 level via the 7^3S_1–6^3P_1 transition at 435.8 nm. LIF signals were detected by two PMTs. The amplified LIF signals were transferred to a digital oscilloscope (Tektronix TDS520C) and the integrated signal area was transferred to a computer for further analysis. For each excitation configuration the LIF signal was monitored at two different wavelengths corresponding to the 7^3S_1–6^3P_2 transition at 546.1 nm and the 6^1P_1–6^1S_0 transition at 184.9 nm. The four combinations of laser excitation and detection wavelength that were used are shown in Fig. 1.

The fluorescence at 184.9 nm was focused with a CaF_2 lens onto the entrance window of a solar blind PMT. The low sensitivity of the PMT above 200 nm allowed operation of the PMT without a filter to reduce scattered laser light and precluded detection of fluorescence at longer wavelengths. As a consequence, the 184.9 nm LIF signal was nearly free of any background noise. A quartz lens was used to focus the fluorescence at 546.1 nm onto a UV-Vis PMT. A filter package with a cutoff filter and a 546 nm interference filter was used to discriminate against scattered laser stray light. The 253.7 nm excitation beam was produced by the frequency doubled output of a Nd:YAG pumped dye laser with a maximum output power in the range of about 1.3 mJ. The sequential excitation beam at 407.8 or 435.8 nm, was produced by a frequency doubled optical parametric oscillator (OPO; Spectra Physics, MOPO) pumped by a Nd:YAG laser (Spectra Physics, Pro 270). The optical parametric oscillator allowed fast switching between the two wavelengths without changing the alignment or the experimental conditions. The maximum output powers at 407.8 and 435.8 nm were in the range of 1.6 and 1.3 mJ, respectively. The line-widths of the fundamental of the dye laser and the frequency doubled outputs of the OPO were measured with a wavemeter. The dye laser fundamental had a line-width of 0.08 cm^{-1}. The frequency doubled OPO outputs at 407.8 and 435.8 nm had line-widths of 0.3 cm^{-1}. Each beam was passed through a telescope to adjust the beam diameters for optimum overlap and maximum sensitivity.

2.2. Kinetics studies

Our experimental approach has been described in detail elsewhere [11] and utilized the PLP-PLIF technique to

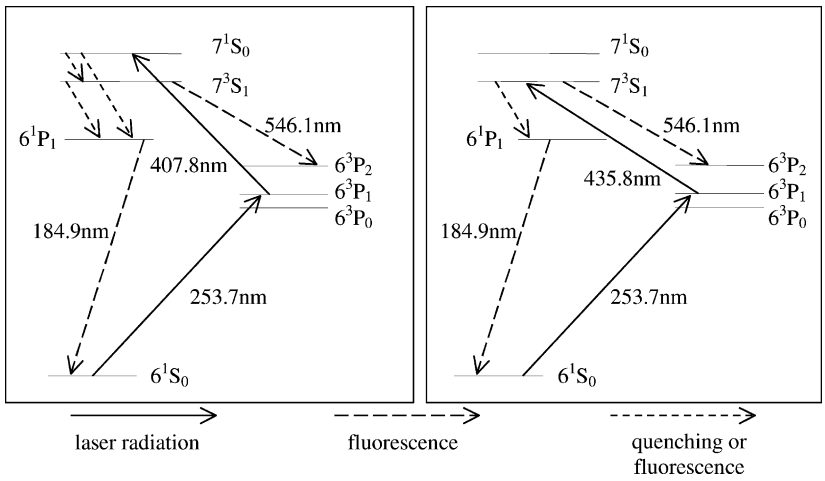

Fig. 1. Relevant energy levels of Hg(0). Laser-excited transitions are shown as solid lines. The sequential two-photon LIF transitions are shown as dashed lines.

measure temporal profiles of OH under pseudo-first-order conditions with mercury as the excess reactant. OH radicals were produced by photolysis of a precursor, HNO_3, in a Pyrex reaction chamber using the 266 nm fourth harmonic output from a Nd:YAG laser.

$$HNO_3 + h\nu_{266\,nm} \rightarrow OH + NO_2 \quad (4)$$

The reaction vessel had two side arms for the observation of LIF and the OH and Hg(0) concentrations were monitored simultaneously. The Hg(0) was monitored by exciting the 6^3P_1–6^1S_0 transition at 253.7 nm, generated by a frequency doubled optical parametric oscillator. OH radicals were excited at ~282 nm via the A–X (1–0) transition followed by observation of fluorescence from the (1–1) and (0–0) bands at 308–316 nm. The excitation laser was a frequency doubled dye laser. Kinetic information was obtained by varying the delay between the photolysis and the probe lasers using a digital delay generator. Experiments were carried on under "slow-flow" conditions. Flows were monitored using calibrated mass flow meters. Because of the low vapor pressure of Hg(0), we measured the decay of OH in the presence and absence of the maximum concentration of Hg(0) we could generate flowing the gas mixture through a thermostated bubbler containing mercury. Since we were unable to observe any evidence for reaction we did not vary the Hg(0) concentrations. For the He measurements, we assumed saturation of the gas flow. For the measurements in air, we monitored the Hg(0) concentration in situ by UV photometry using the 253.7 nm lines from a Hg lamp, an absorption cell and a bandpass filter/photomultiplier combination. The effective absorption cross-section with our Hg lamp was determined using same Hg lamp and bandpass filter and monitoring the attenuation due to a calibrated source of Hg(0). The value that we obtained was $2.1 \times 10^{-14}\,cm^{-2}$.

3. Results

3.1. Linearity and sensitivity

All data shown here were corrected for background stray light and electronic noise. First, the LIF signal was measured with both excitation beams present, then one laser was blocked to measure the background from the other beam. With detection at 184.9 nm, it was found that only the 253.7 nm excitation beam gave a scattered light signal and then only when the PMT was at the very high voltage that was used for low concentration measurements, no scattered light could be detected from the 407.8 or 435.7 nm beams. Therefore, the background for this detection scheme was measured by blocking the 407.8 or 435.7 nm beams. With detection at 546.1 nm, the 253.7 nm scatter was totally blocked by the filters and only the blue lasers were responsible for scattered light. Therefore, the background was measured with the 253.7 nm beam blocked and only the blue lasers present.

A complete set of measurements with all four combinations of the two excitation wavelengths and two detection wavelengths was performed. As Fig. 1 shows, 435.8 nm excitation leads directly to the energy level, 7^3S_1, that fluoresces at 546.1 nm, while observation of 184.9 nm fluorescence requires collisional energy transfer to the 6^1P_1 level which lies approximately $8300\,cm^{-1}$ below 7^3S_1. With sequential excitation of the 7^1S_0 level at 407.8 nm observation of fluorescence at 184.9 nm requires population of the 6^1P_1 level via an allowed radiant transition at 1014 nm or via collisional energy transfer. Observation of fluorescence at 546.1 nm requires collisional energy transfer to the 7^3S_1 level which lies approximately $1600\,cm^{-1}$ below the 7^1S_0 level. The Hg concentration ranged from 1 to 14,000 $ng\,m^{-3}$ in nitrogen buffer gas. The integration time for all measurements was 10 s or 100 laser pulses per data point. Fig. 2a–f

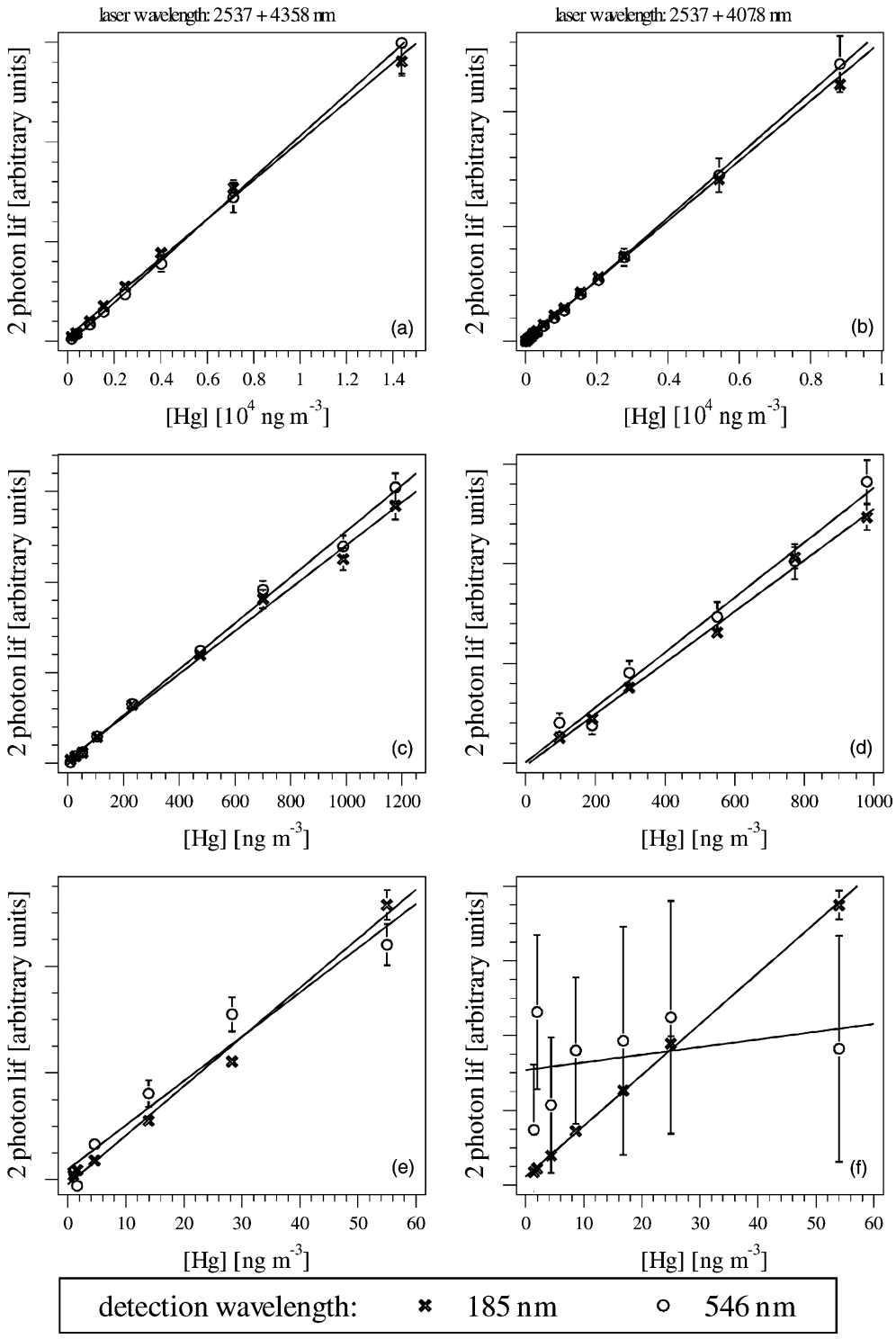

Fig. 2. Linearity curves for all four variants of the sequential two-photon excitation schemes used in this work.

shows curves using either 407.8 or 435.7 nm for the second excitation step. In each case, the relative LIF signal at 184.9 and 546.1 nm is shown with the signals arbitrarily normalized to each other to appear on the same scale. For concentrations above 1000 ng m^{-3}, all four excitation/detection combinations give a linear response with no significant differences between the configurations. At these mercury concentrations, laser scattered light was much lower than the LIF signals at 546.1 and 184.9 nm. Fig. 2c and d shows similar linearity curves but at concentration values below 1200 ng m^{-3}. In each case, a linear relationship with concentration is observed, but the increased level of scattered

light relative to the fluorescence signal starts to become apparent for 546.1 nm detection. If the 546.1 nm line is monitored, direct excitation to the fluorescing 7^3S_1 level gives a much stronger fluorescence signal than 407.8 nm excitation and hence better sensitivity as is seen in Fig. 2c. Using direct excitation at 435.8 nm the magnitude of the fluorescence signal is twice the magnitude of the scattered laser at a concentration of approximately 10 ng m^{-3} whereas with excitation at 407.8 nm this signal-to-noise ratio is reached at approximately 100 ng m^{-3}, and this configuration is not adequate for detection at lower concentrations.

At concentrations below 60 ng m^{-3}, shown in Fig. 2e, excitation at 435.8 nm, gave linear LIF signals down to 1 ng m^{-3} for both detection wavelengths, however the scatter in the 546.1 nm data is greater. Using the 7^1S_0–6^3P_1 transition at 407.8 nm, no signal is observed above the noise at 546.1 nm; however, with 184.9 nm detection, the signal is linear down to 1 ng m^{-3}, the lowest concentration that we could generate with our dilution system. Excitation at 407.8 nm produces a much stronger fluorescence signal at 184.9 nm relative to 435.8 nm excitation and this is reflected in the precision of the 184.9 nm linearity curve in Fig. 2f. In addition, the precision and essentially no offset in this line indicate that both the Tekran and sequential two-photon techniques show an extremely linear response and that any "instrumental offset" in the Tekran is extremely small. In summary, excitation at 435.8 nm produces stronger fluorescence signal at 546.1 nm than at 184.9 nm, however since the background is much lower at the latter wavelength, both detection wavelengths show similar precision. In contrast, 407.8 nm excitation produces a strong fluorescence signal at 184.9 nm and a much weaker signal at 546.1 nm. Because of the very low scattered light background at 184.9 nm, this approach gives the best precision and the best sensitivity of the four configurations.

A calculation of limits of sensitivity requires a statistical analysis of the fluctuations in the background scattered laser light and electronic noise. Since the linearity tests were based on 10 s integrations they provide a limited data set for statistical analysis of sensitivity. A comparison of the relative sensitivities can be obtained by comparing the mercury concentrations at which the magnitude of the fluorescence signal was twice the magnitude of the scatter and this is shown in Table 1 for 10 s integration times.

Table 1
Estimated sensitivities of two-photon LIF schemes for detection of Hg(0) in N_2 with a 10 s integration time

Second excitation wavelength (nm)	LIF detection wavelength (nm)	Detection limit (ng m^{-3})
407.8	184.9	0.1
407.8	546.1	150
435.8	184.9	5
435.8	546.1	20

All schemes use 253.7 nm for the initial excitation step.

Since sequential excitation at 407.8 nm produced the best results further sensitivity tests were performed at a concentration of 4 ng m^{-3}, as measured by the Tekran, and these are described elsewhere [9]. The limit of detection, which we define as being the Hg(0) concentration which produces an LIF signal equal to the 2σ deviation in the background, is 0.4 ng m^{-3} for a 1 s integration and 0.1 ng m^{-3} for a 10 s integration in N_2 buffer gas.

In single photon LIF, the detection sensitivity is limited by the ratio of detected resonance fluorescence to laser scatter. In this case, the experimental configuration and attempts to minimize scatter are particularly critical and any determination of sensitivity will tend to laboratory specific. In addition, sensitivity will be maximized by working at low laser powers so that the fluorescence is linear with laser power. As shown in Fig. 3, this requires operation at very low powers. We found that single photon LIF was inferior to sequential two-photon techniques for detection at low levels and a concentration of 500 ng m^{-3} in air at an integration time of 10 s, gave adequate signal-to-noise for kinetic or spectroscopic measurements.

3.2. Characterization of flux and line-width effects

3.2.1. Saturation

Changing the laser diameter effects two important parameters of the measurement. Increasing the diameter increases the detection volume and thus the number of mercury atoms that are sampled. On the other hand, it reduces the laser flux. At low fluxes, the LIF signal is proportional to laser power, partial or full saturation makes the system potentially less sensitive to fluctuations in the laser power and to quenching effects. However, in a complex multilevel system losses to ionization or transfer to non-fluorescing levels will complicate this process. We obtained optimum sensitivity with a diameter of about 5 mm, equivalent to a fluence of about 5 mJ cm^{-2} for the laser at 253.7 nm and 6–7 mJ cm^{-2} for the lasers at 407.8 or 435.8 nm. We examined the saturation characteristics using both single and sequential excitation. Fig. 3 shows the single photon saturation curve, exciting only the 6^3P_1–6^1S_0 transition at 253.7 nm with resonance fluorescence detection. Very low powers, less than 10 μJ per pulse, were required to obtain a linear response and the transition appears to be fully saturated at approximately 0.5 mJ corresponding to a fluence of 2.5 mJ cm^{-2}. Fig. 4 shows the saturation response with sequential two-photon pumping at 253.7 and 407.8 nm with detection at 184.9 nm. The 253.7 nm laser power was fixed at 0.8 mJ per pulse and the variation of the LIF signal, shown as (●), as a function of 407.8 nm power was monitored. The transition appears to saturate at approximately 1 mJ per pulse. In a second experiment, the 407.8 nm power was fixed at 1.6 mJ per pulse and the LIF signal, shown as (+), was monitored as a function of 253.7 nm power. While the LIF signal is partially saturated it clearly has not reached full saturation. The higher laser fluence that is necessary to saturate the first step in

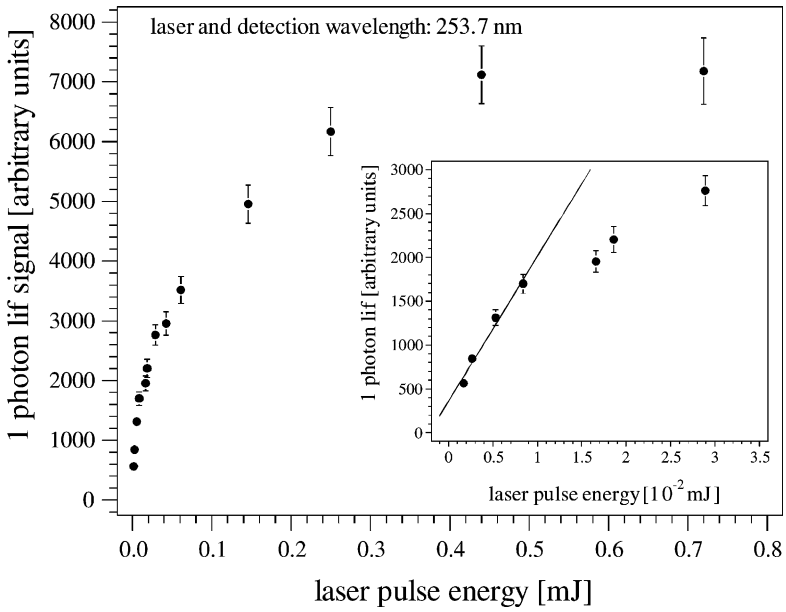

Fig. 3. Saturation curve for single photon excitation of Hg(0) via the 6^3P_1–6^1S_0 transition. Inset shows expansion in low power region.

the two-photon LIF measurement, can be explained by the fact that the second laser is depopulating the 6^3P_1 state and higher photon densities are necessary to reach equal population of the 6^3P_1 and 6^1S_0 states.

3.2.2. Excitation line profiles

Fig. 5 shows 253.7 nm single photon excitation line profile with excitation and detection at 253.7 nm. The line scans are done at 0.2 and 1.1 mJ and show the power broadening of the line-width from a FWHM of 0.008–0.015 nm. The line-width at 0.2 mJ per pulse corresponds to a line-width of 1.2 cm^{-1} which is a reasonable convolution of the estimated laser line-width of 0.16 cm^{-1} and the natural line-width of the 6^3P_1–6^1S_0 transition which is approximately 0.8 cm^{-1} as a result of the hyperfine components from the different Hg isotopes.

Fig. 6 shows a scan of the second excitation laser over the 407.8 nm line, while the laser for the first excitation step was fixed to the center of the line at 253.7 nm. The two curves show the LIF signal measured at the two different

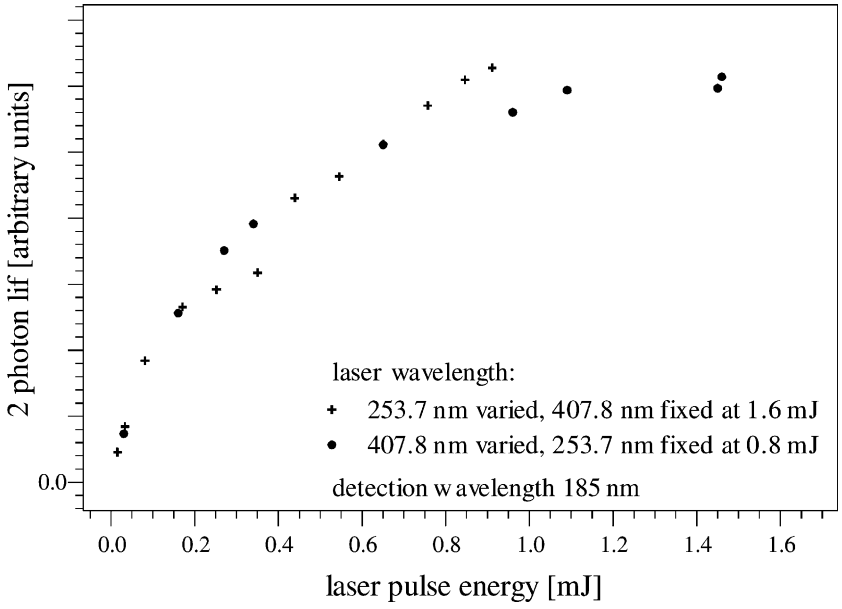

Fig. 4. Saturation curve for sequential two-photon excitation via the 6^3P_1–6^1S_0 and 7^1S_0–6^3P_1 transitions. The filled circles (●) show the variation in the LIF signal as a function of 407.8 nm energy with the 253.7 nm energy fixed at 0.8 mJ. The crosses (+) show the variation in the LIF signal as a function of 253.7 nm energy with the 407.8 nm energy fixed at 1.6 mJ.

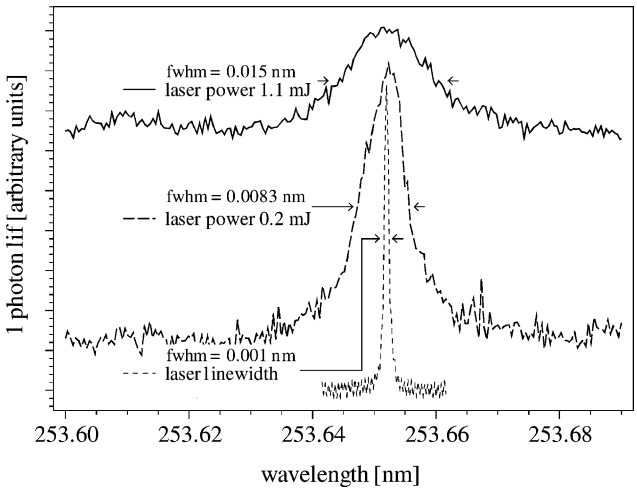

Fig. 5. Line-width of the single photon 6^3P_1–6^1S_0 transition at two laser energies. The line-width of the excitation laser at 253.7 nm is also shown.

detection wavelength at 184.9 and 546.1 nm, together with the laser line-width as measured by the wavemeter. The noise level at 546.1 nm is higher because of the laser stray light. The line-width is in the range of 0.05 nm, the line-width of the laser is much smaller, and it can be seen that the line-width is again dominated by the hyperfine components of the different isotopes.

Fig. 7 shows a similar measurement with the second excitation laser tuned over the 7^3S_1–6^3P_1 transition, again the measured 435.8 nm laser line-width is included for comparison. It can be seen that the line-width of this transition is extremely broad and unsymmetrical. The asymmetry makes it difficult to define a FWHM but the line extends over about 0.8 nm. The observed lineshape is very similar to one reported in a saturated LIF study of Hg (6^3P_1) in a high-pressure metal halide discharge lamp [12]. In that work, Hg (6^3P_1) was generated by the lamp discharge and monitored by both saturated LIF and optogalvanic spectroscopy. The excitation line profiles that were obtained show the same asymmetry and very broad line-width that we report here. Again, this may be due to the isotopic and hyperfine splitting of the 7^3S_1 level of mercury.

3.2.3. Quenching and laser synchronization

At atmospheric pressure the synchronization between the sequential excitation laser pulses is quite critical. Fig. 8 shows the LIF signal as a function of the delay between the two laser pulses. The shape of the temporal profile in Fig. 8 is a convolution of the temporal pulses of the exciting lasers and the lifetime of the 6^3P_1 level and is not symmetrical. In practice the delay was adjusted to maximize the LIF signal. It can be seen that a small shift in the delay can produce a significant drop in the signal. It suggests that the jitter between the two excitation pulses needs to be less than 1 ns to maximize sensitivity and measurement precision.

Since our detection scheme involves three electronically excited states, we would expect the fluorescence quantum yield to be sensitive to the identity and pressure of the buffer gas. Quenching of the 6^3P_1 level has been well studied and O_2 is found to be a particularly efficient quencher with a rate coefficient of 3.57×10^{-10} cm^3 molecule^{-1} s^{-1} [13], about 20 times faster than N_2 [14], and both He and Ar are inefficient quenchers [14]. We are not aware of any work on the quenching of the 7^1S_0 or 6^1P_1 levels. Based on the reported quenching rate in O_2, we would expect a lifetime of less than 1 ns for the 6^3P_1 level and this is reflected in Fig. 8. The dependence of the 6^1P_1–6^1S_0, 184.9 nm LIF

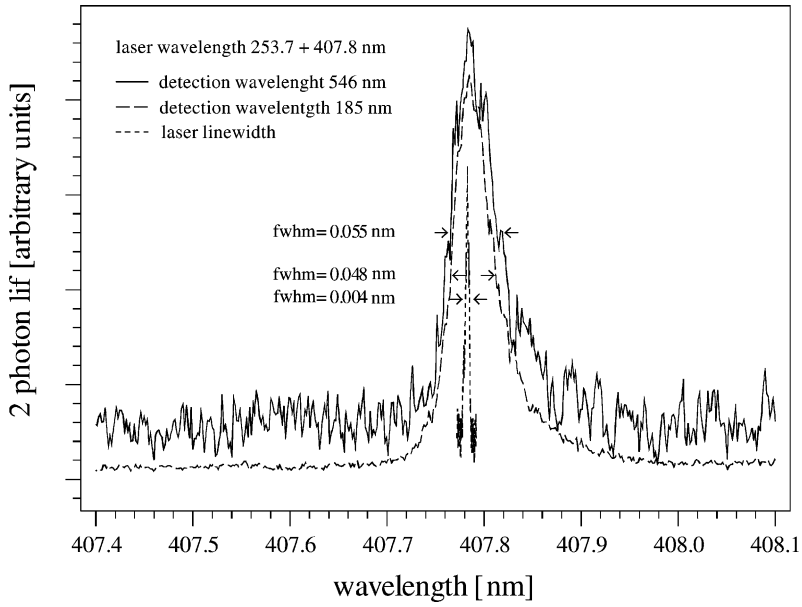

Fig. 6. Line-width of the 7^1S_0–6^3P_1 transition with the 253.7 nm laser fixed. The line-width of the second excitation laser at 407.8 nm is also shown.

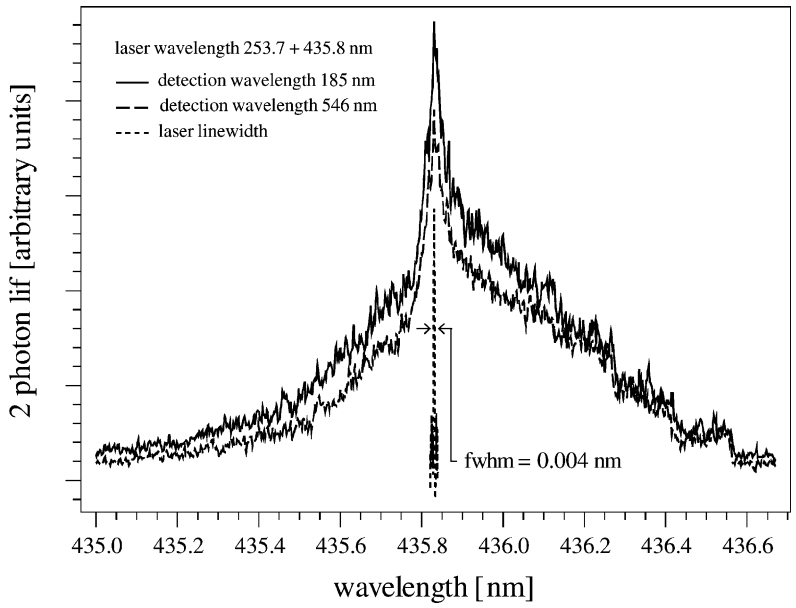

Fig. 7. Line-width of the 7^3S_1–6^3P_1 transition with the 253.7 nm laser fixed. The line-width of the second excitation laser at 435.8 nm is also shown.

signal on pressure and bath gas is a convolution of quenching effects on all three levels. We examined the relative overall quenching efficiencies of N_2, air, He and Ar for the scheme involving 407.8 nm excitation with detection at 184.9 nm and the detailed results have been reported elsewhere [9]. We found that both air and N_2 are very efficient quenchers while Ar and He are not efficient. At atmospheric pressure the fluorescence lifetime essentially follows the shape of the excitation pulse suggesting that the 7^1S_0, 7^3S_1 and 6^1P_1 are all efficiently quenched in air or N_2.

3.2.4. *Effect of flux, line-width and quenching on detection sensitivity*

These studies demonstrate that the detection sensitivity in these schemes is not constrained by the power or spectral characteristics of the excitation lasers. Indeed, they demonstrate that because of the relatively broad line-width of the transitions and the onset of saturation at low laser fluxes that relatively basic dye lasers or OPO's with line-widths of 0.5–1 cm^{-1} and output powers of 1–2 mJ are all that is required to achieve high detection sensitivity. Use of

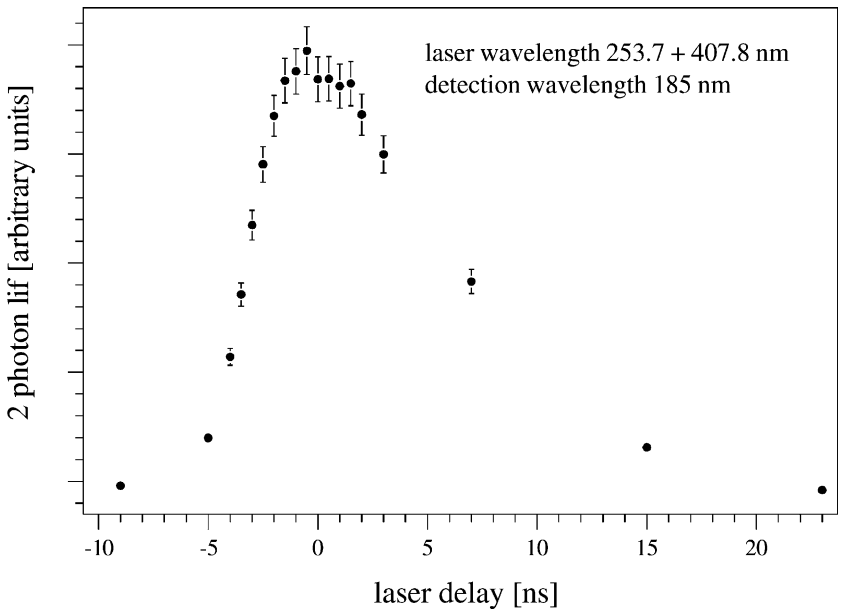

Fig. 8. Two-photon LIF signal as a function of the temporal delay between the excitation laser pulses.

either 407.8 nm or 435.8 nm should give adequate sensitivity for laboratory studies. For ambient monitoring, the 253.7/407.8 nm excitation scheme offers the most sensitive approach and is essentially signal, rather than signal-to-noise limited. Here, the best gain in sensitivity will come from an increase in excitation frequency and a 50 Hz system should be more than adequate to perform eddy correlation measurements on Hg(0) at ambient levels. The use of this approach in conjunction with preconcentration followed by detection in He should offer a large increase in sensitivity, albeit with some loss of temporal resolution.

We have discussed the currently available techniques for ambient measurements [9], all of which utilize preconcentration on gold tubes and are typically coupled with cold vapor atomic fluorescence spectrophotometry (CVAFS). Use of sequential two-photon excitation in conjunction with preconcentration followed by desorption and detection in He bath gas would offer at least 2 orders of magnitude in detection sensitivity albeit with some loss in temporal resolution. Rodgers et al. first proposed the use of sequential two-photon LIF for the detection of Hg(0) using the excitation scheme involving the 6^3P_1–6^1S_0 and 7^1S_0–6^3P_1 transitions with detection at 184.9 nm [15]. They reported a detection limit of 1×10^9 atoms cm^{-3} in N_2 with a integration time of 15 min using a 10 Hz laser system. In more recent, work Resto et al. [16] demonstrated sequential two-photon excitation on the 6^3P_1–6^1S_0 and 7^3S_1–6^3P_1 transitions with detection at 546.1 nm. They report detection of 100 pg of Hg, monitoring chemically bound mercury using electrothermal atomization and claim the much lower detection limit of 90 fg. Hg(0) detection using cavity ring-down spectroscopy [17–19] has also been reported but at concentration levels which significantly exceed naturally occurring background levels.

3.3. Kinetics of Hg(0) with OH

As noted above, our ability to study this reaction by monitoring the decay of OH in a pseudo-first-order excess of reactant was limited by the low vapor pressure of Hg(0), $\sim 5.5 \times 10^{13}$ molecules cm^{-3} at 25 °C. In these experiments, we observed the decay of OH in the presence and absence of Hg(0) in He and air buffer gases at room temperature. Hg(0) was monitored simultaneously using LIF and remained constant during the experiments. The initial OH concentration was less than 1×10^{12} molecules cm^{-3} so pseudo-first-order conditions applied. Table 2 summarizes the results of multiple measurements of the OH decay rates that we obtained in the presence and absence of Hg(0). From the data in air, we can take the difference between 1σ upper limit on the pseudo-first-order rate in the presence of Hg(0), $(186 + 3 = 189\,s^{-1})$, and the 1σ lower limit in the absence of Hg(0), $(189 - 5 = 184\,s^{-1})$ giving an uncertainty of $5\,s^{-1}$ increase in the pseudo-first-order rate at a concentration of 4.1×10^{13} molecules cm^{-3}. This gives an upper limit of 1.2×10^{-13} cm^3 $molecule^{-1}$ s^{-1} for the rate coefficient. We saw no evidence for an equilibration between OH and Hg(0) which allows us to place an upper limit on the equilibrium constant for HgOH formation of $K_c = 5 \times 10^{-16}$ cm^3 $molecule^{-1}$. The low Hg(0) concentration precludes a better estimate and this limit would correspond to a strongly bound complex. In fact, the equilibrium constant, if equilibrium exists is probably much lower. As we note above, any reaction must occur via the formation of a complex which subsequently reacts with O_2. In the case of CS_2, which reacts with OH via formation of a CS_2OH complex followed by reaction of the complex with O_2 [20,21], the CS_2OH equilibrium constant has a value of $K_c = 1 \times 10^{-17}$ cm^3 $molecule^{-1}$ at 298 K [21]. This is adequate to produce an effective rate of $\sim 1 \times 10^{-12}$ cm^3 $molecule^{-1}$ s^{-1} for the reaction of OH with CS_2 in one atmosphere of air at 298 K. Hence, our value of K_c does not constrain the upper limit of the effective rate coefficient for a mechanism based on reactions (1b) and (2) at 298 K.

Table 2
Measured pseudo-first-order rates of OH in the presence and absence of Hg(0) in air and He buffers

Pseudo-first-order rate ($\pm 1\sigma$)	Buffer gas	[Hg(0)] (molecules cm^{-3})
$189 \pm 5\,s^{-1}$	Air (400 Torr)	0
$186 \pm 3\,s^{-1}$	Air (400 Torr)	4.1×10^{13}
$262 \pm 5\,s^{-1}$	He (100 Torr)	0
$263 \pm 6\,s^{-1}$	He (100 Torr)	5×10^{13}

In an initial report of our kinetic studies to the Florida Department of Environmental Protection (FDEP) [22], we reported an upper limit of 5×10^{-13} cm^3 $molecule^{-1}$ s^{-1} for reaction (1) in He. These results were circulated by the FDEP and we became aware of another study of reaction (1) performed by Sommar et al. [23] at the University of Goteborg, which used a competitive rate technique and measured a much faster rate coefficient of $(2.6 \pm 1.5) \times 10^{-12}$ cm^3 $molecule^{-1}$ s^{-1} [24]. At their request, the details of our work were communicated to the Goteborg group and further experiments were undertaken in our laboratory in an effort to resolve the discrepancy. Sommar et al. [25] have recently published a much slower rate coefficient of $(8.7 \pm 2.8) \times 10^{-14}$ cm^3 $molecule^{-1}$ s^{-1} for reaction (1), in agreement with our work but do not discuss in detail their previous reports or our results. Bergan and Rodhe [5] have used a global mercury model to evaluate the potential role of hydroxyl-initiated oxidation of Hg(0). They find that the new rate coefficient reported by Sommar et al. gives an Hg(0) lifetime of 130 days with respect to removal by OH. This would make the OH reaction one of the dominant removal mechanisms for Hg(0). Bergan and Rodhe concluded that this rate is not consistent with observed atmospheric concentrations but that OH may be an important oxidant. If the rate coefficient reported by Sommar et al. is accurate, we should have observed a $5\,s^{-1}$ increase in our pseudo-first-order rates in air in the presence of Hg(0) and this lies at the limit of the precision of our measurements. We are planning to undertake measurements which should allow us to better define

the upper limit and measure the temperature dependence of the rate coefficient. It should be noted that if this reaction proceeds by a complex mechanism, it could show a dramatic increase in the effective rate in air at lower temperature. This type of behavior is observed in the reactions of OH with CS_2 [20,21] and DMS [26,27]. In each of these cases, reaction proceeds via the formation of a weakly bound complex which subsequently reacts with O_2.

4. Conclusions

We have evaluated four variants of detection schemes for Hg(0) based on sequential two-photon laser-induced fluorescence. All four variants show an extremely large dynamic range. An excitation scheme involving the 6^3P_1–6^1S_0 and 7^1S_0–6^3P_1 transitions at 253.7 and 408.7 nm coupled with detection at 184.9 nm shows the greatest sensitivity. Using this approach, our limits of detection with optimized fluorescence detection are 0.4 ng m^{-3} with a 1 s integration time and 0.1 ng m^{-3} with a 10 s integration time in air. Detection limits in He are a factor of 50 lower. We have examined a variety of effects which will affect sensitivity, including line-width, saturation and fluorescence quenching. We have measured the decay of the hydroxyl radical in an excess of gas phase mercury. We were unable to observe any evidence for reaction and report an upper limit of 1.2×10^{-13} cm^3 $molecule^{-1}$ s^{-1} for the rate coefficient.

Acknowledgements

This work was supported by the Florida Department of Environmental Protection. We thank Tom Atkeson and Bob Stevens for the loan of the Tekran 2537A and for their interest in this work.

References

[1] National Research Council (NRC) Toxicological Effects of Methylmercury, National Academy Press, 2000.
[2] R. Ebinghaus, S.G. Jennings, W.H. Schroeder, T. Berg, T. Donaghy, J. Guentzel, C. Kenny, H.H. Kock, K. Kvietkus, W. Landing, T. Muhleck, J. Munthe, E.M. Prestbo, D. Schneeberger, F. Slemr, J. Sommar, A. Urba, D. Wallschlager, Z. Xiao, Atmos. Environ. 33 (1999) 3063.
[3] S.E. Lindberg, Atmos. Environ. 14 (1980) 227.
[4] C.J. Lin, S.O. Pehkonen, Atmos. Environ. 33 (1999) 2067.
[5] T. Bergan, H. Rodhe, J. Atmos. Chem. 40 (2001) 191.
[6] W.H. Schroeder, K.G. Anlauf, L.A. Barrie, J.Y. Lu, A. Steffen, D.R. Schneeberger, T. Berg, Nature 394 (1998) 331.
[7] S.E. Lindberg, S. Brooks, C.-J. Lin, K.J. Scott, M.S. Landis, R.K. Stevens, M. Goodsite, A. Richter, Environ. Sci. Technol. 36 (2002) 1245.
[8] G. Yarwood, H. Niki. A critical review of available information on transformation pathways for mercury species in the atmospheric environment, Atmospheric Environment Service, Downsview, Ontario, Canada, 1990.
[9] D. Bauer, P. Campuzano-Jost, A.J. Hynes, J. Environ. Monit. 4 (2002) 339.
[10] Tekran, 132 Railside Road, Unit 1, Toronto, Canada M3A 1A3.
[11] L. D'Ottone, P. Campuzano-Jost, D. Bauer, A.J. Hynes, J. Phys. Chem. 105 (2001) 10538.
[12] J. Kramer, J. Appl. Phys. 67 (1990) 2289.
[13] J.V. Michael, G.N. Suess, J. Phys. Chem. 78 (1974) 482.
[14] A.C.G. Mitchell, M.W. Zemansky, Resonance Radiation and Excited Atoms, University Press, London, 1961.
[15] M.O. Rodgers, J.D. Bradshaw, K. Liu, D.D. Davis, Opt. Lett. 7 (1982) 359.
[16] W. Resto, R.G. Badini, B.W. Smith, C.L. Stevenson, J.D. Winefordner, Spectrochim. Acta Part B 48 (1993) 627.
[17] R.T. Jongma, M.G.H. Boogaarts, I. Holleman, G. Meijer, Rev. Sci. Instrum. 66 (1995) 2821.
[18] S.Q. Tao, F.J. Mazzotti, C.B. Winstead, G.P. Miller, Analyst 125 (2000) 1021.
[19] S. Spuler, M. Linne, A. Sappey, S. Snyder, Appl. Opt. 39 (2000) 2480.
[20] B.M.R. Jones, J.P. Burrows, R.A. Cox, S.A. Penkett, Chem. Phys. Lett. 88 (1982) 372.
[21] A.J. Hynes, P.H. Wine, J.M. Nicovich, J. Phys. Chem. 92 (1988) 3846.
[22] A.J. Hynes, Laboratory Studies of Atmospheric Mercury Transformation, Quarterly Report for the Period 8/1/97–10/31/97, Florida Department of Environmental Protection, Tallahassee, Florida.
[23] J. Sommar, K. Gardfeldt, X. Feng, O. Lindqvist, Rate coefficients for gas-phase oxidation of elemental mercury by bromine and hydroxyl radicals, in: Proceedings of the 5th International Conference on Mercury as a Global Pollutant, Rio de Janeiro, Brazil, 1999.
[24] A. Ryaboshapko, I. Ilyin, R. Bullock, R. Ebinghaus, K. Lohman, J. Munthe, G. Petersen, C. Seigneur, I. Wängberg, Intercomparison Study of Numerical Models for Long-Range Atmospheric Transport of Mercury, MSC-E Technical Report 2/2001, Meteorological Synthesizing Centre—East, Moscow, Russia.
[25] J. Sommar, K. Gardfeldt, D. Stromberg, X.B. Feng, Atmos. Environ. 35 (2001) 3049.
[26] A.J. Hynes, P.H. Wine, D.H. Semmes, J. Phys. Chem. 90 (1986) 4148.
[27] M.B. Williams, P. Campuzano-Jost, D. Bauer, A.J. Hynes, Chem. Phys. Lett. 344 (2001) 61.